

Observation of inverse Čerenkov interaction between free electrons and laser light

J. A. Edighoffer, W. D. Kimura, R. H. Pantell, M. A. Piestrup, and D. Y. Wang

Department of Electrical Engineering, Stanford University, Stanford, California 94305

(Received 18 August 1980)

Momentum exchange was observed between laser light and an electron beam using the inverse Čerenkov effect. This interaction was accomplished by introducing a gas with an index of refraction which reduced the phase velocity of the light wave to match the velocity of the electron. A 30-MW Nd:YAG 1.06- μm laser intersected 102-MeV electrons at an angle of 18 mrad in hydrogen gas. The beams overlapped in the interaction region for approximately 10^5 optical wavelengths. The energy exchange by the inverse Čerenkov effect was verified in two ways: First, a change was observed in the electron energy distribution in the presence of the laser, and second, this change was observed to be a function of the index of refraction, as determined by the pressure of the gas. A $\pm 13\%$ variation about the pressure for optimum energy exchange reduced the interaction by one-half. The results of the experiment agree with the predictions of a Monte Carlo computer simulation of the interaction. Methane gas was also investigated as a phase-matching medium. Possible applications include laser-driven particle accelerators and stimulated Čerenkov devices, such as optical klystrons and traveling wave tubes.

I. INTRODUCTION

The very high electric fields associated with laser light has generated a considerable amount of interest in the possibility of designing laser-driven particle accelerators.¹⁻⁵ Laser light can also be used to modulate the momentum of an electron beam,⁶⁻¹⁰ generating electron bunches separated by an optical wavelength. In a manner analogous to microwave devices, optical klystrons^{11,12} or traveling wave tubes¹³⁻¹⁶ could then be devised, which would extract energy from the bunched beam.^{17,18}

In these devices, significant energy exchange between laser light and free electrons is necessary. This means a method of maintaining phase-matching over sizable distances is required. The experiment reported here used the inverse Čerenkov^{6,19} effect to achieve energy exchange. In the inverse Čerenkov effect, the phase velocity of a light wave in a medium is $v_L = c/n$, where c is the velocity of light and n is the index of refraction of the medium (see Fig. 1). An electron traveling with velocity v_e intersects the laser beam at an angle θ . To insure the electron will remain in a field of constant phase, the phase velocity component of the light in the direction of the electron's velocity $v_L/\cos\theta = c/n \cos\theta$, must equal the velocity of the electron, βc , where $\beta = v_e/c$. This results in the angle $\theta = \cos^{-1}(1/n\beta)$, which is recognized to be the Čerenkov condition associated with Čerenkov radiation.

An earlier preliminary investigation⁶ of the inverse Čerenkov effect used a different experimental system with helium gas as the phase-matching medium; whereas in the present experiment hydrogen and methane gases were used. The small signal-to-noise measurements of the pre-

vious work relied on spatial mismatch between the two intersecting beams to verify the effect. In the experiment reported here, there was positive demonstration of interaction between electrons and laser light by the inverse Čerenkov mechanism. It was demonstrated in two ways: First, a change was observed in the electron energy distribution in the presence of the laser and second, this change was observed to be a function of the index of refraction as determined by the Čerenkov condition.

Assuming the laser beam to be a plane wave with a Gaussian intensity variation, the effect of the electric field on the electron's momentum has been calculated.⁶⁻⁸ For perfect phase-matching and a single transit of the electron through the laser beam, the maximum energy exchange is given by

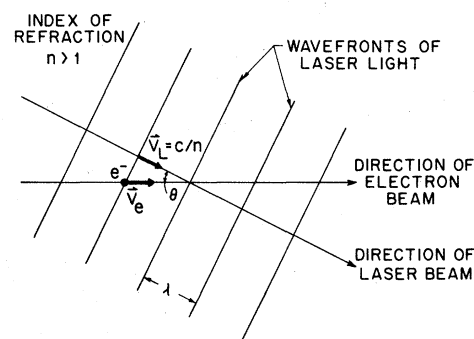


FIG. 1. Inverse Čerenkov phase-matching scheme. The phase velocity of the laser light propagating through a medium with index of refraction $n > 1$ is $v_L = c/n$, where c is the speed of light. An electron traveling with velocity v_e will remain in a field of constant phase provided it intersects the laser beam at an angle $\theta = \theta_c = \cos^{-1}(1/n\beta)$, where θ_c is the Čerenkov angle and $\beta = v_e/c$. The wavelength of the laser is λ .

$$\Delta W_{\max} (\text{keV}) = 38.8 [P(\text{MW})]^{1/2}, \quad (1)$$

where ΔW_{\max} is the maximum possible change in energy of the electron and P is the peak power of the laser in megawatts. This maximum energy exchange is independent of wavelength, electron energy, laser waist size, and the Čerenkov angle. The same result is obtained using a laser beam synthesized by an angular summation of plane waves forming a Gaussian waist.

The efficiency of momentum exchange is reduced by electron-beam divergence and collisions within the medium. Owing to divergence, only a portion of the electrons in the beam will intersect the laser at the Čerenkov angle; the others will slip in phase with respect to the electromagnetic wave. Electrons will still experience a significant amount of energy exchange if their directions of motion are within an angular range equal to the laser divergence (in this experiment, ≈ 0.5 mrad). Collisions generate random energy loss and also alter the direction of the electrons, causing them to lose phase-matching within the interaction region. These effects do not change the value of ΔW_{\max} , but rather reduce the number of electrons that experience this large energy change. A Monte Carlo computer simulation, which was developed to study the interaction process, incorporates the effects of collisions, electron- and laser-beam divergences, electron energy distributions, and electron- and laser-beam widths. The computer results will be presented and compared with the experimental data.

II. EXPERIMENTAL METHOD

Figure 2 is a simplified schematic depicting the topview of the experimental system. The electrons, generated by Stanford's Superconducting Accelerator (SCA), entered the evacuated beamline pipe from the left. Various steering magnets and a set of focusing quadrupole magnets were used to position and focus the beam into the gas cell on the right where the inverse Čerenkov interaction occurred.

The laser system was situated on a table below the beamline with the light guided and focused into the interaction region by a series of mirrors and lenses. The Nd:YAG oscillator and amplifier delivered 30 MW of 8-nsec pulsed $1.06\text{-}\mu\text{m}$ radiation to the gas cell, which corresponded to a peak electric field of $\approx 10^6$ V/cm or a peak acceleration gradient of ≈ 2 MeV/m. Substitution into (1) with $P=30$ MW, shows that the maximum energy exchange possible was, $\Delta W_{\max}=213$ keV. The same number was calculated by a more accurate laser-field representation and integral procedure in the Monte Carlo computer simulation.

The laser and electron beams were focused to ≈ 1.2 mm (diameter) and ≈ 1.6 mm (diameter) respectively, at the center of the gas cell. The laser beam entered the gas filled interaction region through a quartz disc window tilted at Brewster's angle. In these windows, 1.6-mm holes were covered with 0.025-mm thick beryllium foil, allowing the electrons to enter and exit the gas cell with a minimal amount of scattering. Constraints in the present window design limited the inter-

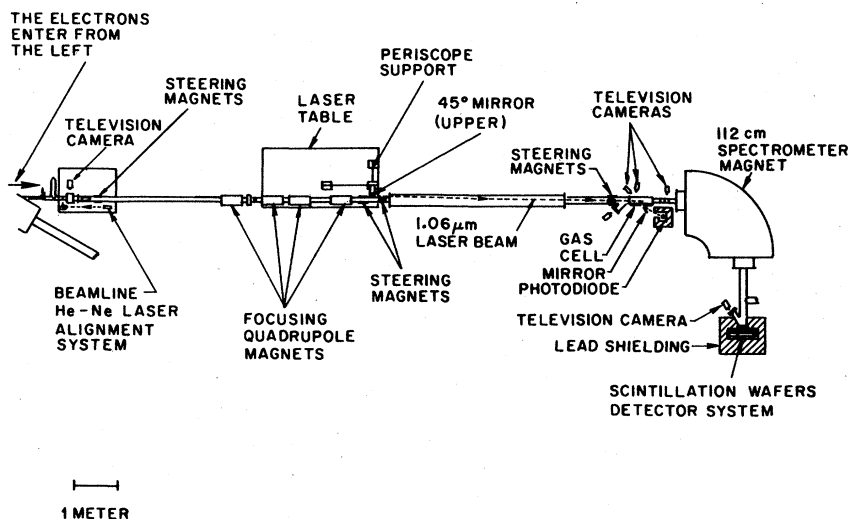


FIG. 2. Simplified schematic depicting the topview of the experimental system. The electrons enter the beamline from the left, interact with the laser in the gas cell on the right, and are detected at the end of the system. The entire experiment is remotely controlled.

TABLE I. System parameters.

Electron Beam	
Source:	Stanford's Superconducting Linear Accelerator (SCA)
Beam energy:	101.8 MeV
Intrinsic energy spread:	$\approx \pm 15$ keV
Width of electron bunches:	9 psec
Bunch separation:	798 psec
Beam spill length:	3 msec
Beam average current (during beam spill):	$60 \mu\text{A}$
Repetition rate:	10 Hz.
Beam divergence (half-angle) in interaction region:	≈ 1.0 mrad
Focused spot size at interaction region:	≈ 1.6 -mm diameter
Laser Beam	
Laser type:	Nd:YAG unstable resonator configuration
Wavelength:	$1.064 \mu\text{m}$
Q-switched pulse length:	8 nsec
Power delivered to interaction region:	30 MW
Beam divergence (half-angle):	0.56 mrad.
Focused spot size at interaction region:	1.2-mm diameter
Linewidth:	0.4 cm^{-1}
Multimode operation	
Interaction Region (Gas Cell)	
Phase-matching mediums:	Hydrogen gas (99.999% pure), Methane gas (99.97% pure)
Interaction angle:	18 ± 1 mrad
Temperature:	19.5°C
Length of gas cell:	41 cm
Length of electron/laser beam overlap:	≈ 7 cm

action angle of the beams to slightly greater than 15 mrad. The electron and laser beams overlapped for about 7 cm, which corresponds to approximately 10^5 optical wavelengths. System parameters are given in Table I.

A crucial parameter in the experiment was the angle the electron and laser beams intersected each other. To determine this, the angle between the laser and the straight-line trajectory through the holes in the windows was measured and found to be 18 ± 1 mrad. A HeNe laser (located on the far left of Fig. 2) was used to align the holes in the windows and thus defined the central trajectory of the electron beam through the gas cell.

The modulation of the electron's momentum was measured with a 90° spectrometer magnet and position detector. The detector consisted of 18 scintillation wafers, each 0.25 mm thick, sandwiched together facing the electron beam edgewise. This detector obtained a pulse-to-pulse energy spectrum with 10.5 keV resolution per wafer.

Figure 3 shows the temporal relationship between the laser pulses, the electron-beam pulses, and the detector sampling gate. The laser emits light every other electron-beam spill; so alternate energy profiles represent modulated and unmodulated electron momentum spectra. A difference

profile is obtained by subtracting unmodulated energy spectra from modulated spectra. This process is illustrated in Fig. 4. The energy spectrum of the electron beam is approximately Gaussian [Fig. 4(a)] without the laser interaction, and becomes flat and broad in the presence of the

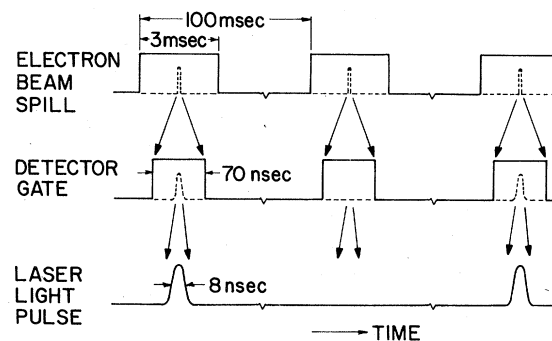


FIG. 3. Temporal relationship between the electron-beam pulses, detector sampling gate, and laser pulses. Not shown in the diagram is the train of 9-psec-long electron bunches, separated by 798 psec, contained within the 3-msec-long beam spill. Thus the 8-nsec laser pulse intersected ≈ 10 bunches; however, the detector gate sampled ≈ 90 bunches which reduced the signal-to-noise ratio.

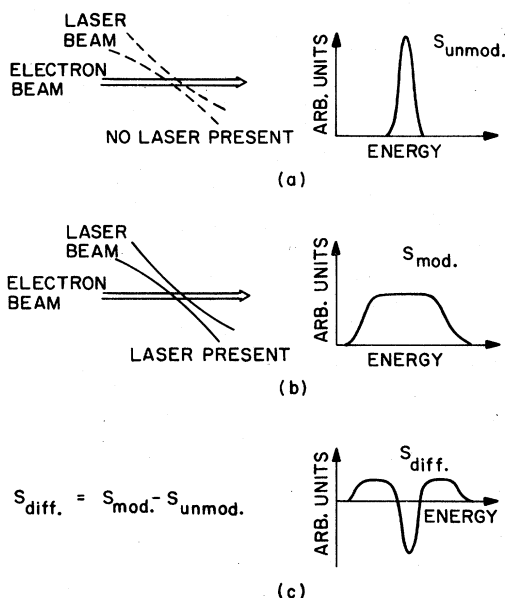


FIG. 4. Schematic of electron energy spectrums. (a) With no laser interaction, the unmodulated electron energy spectrum is approximately Gaussian. (b) With laser interaction, the modulated electron energy spectrum becomes flat and broad. (c) Subtracting the spectrum in (a) from (b) produces a difference spectrum.

laser [Fig. 4(b)]. Subtracting these two spectra generates a difference spectrum [Fig. 4(c)]. The negative central region of this spectrum gives an indication of the number of electrons modulated, and the positive sidelobes indicate the maximum momentum change in the electrons.

A difference spectrum is a sensitive experimental measure of the interaction, since much of the systematic sources of error are cancelled. Systematic errors arise from the electronic components of the laser and the electron accelerator, and from the high background radiation. In addition, the difference spectrum cancels long-term fluctuations in electron-beam current and spectrometer magnet current. Only a fraction of the electrons in the beam spill receive substantial modulation, as most arrive at the wrong time (see Fig. 3) or with the wrong phase space to be properly matched to the laser light.

III. EXPERIMENTAL RESULTS

An unmodulated electron energy spectrum is shown in Fig. 5, for electrons passing through the gas cell filled with hydrogen at 1.28 atm. The full width at half-maximum (FWHM) of the spectrum is approximately 50 keV. The solid curve in Fig. 5 is the unmodulated spectrum produced by the computer simulation program using the same experimental

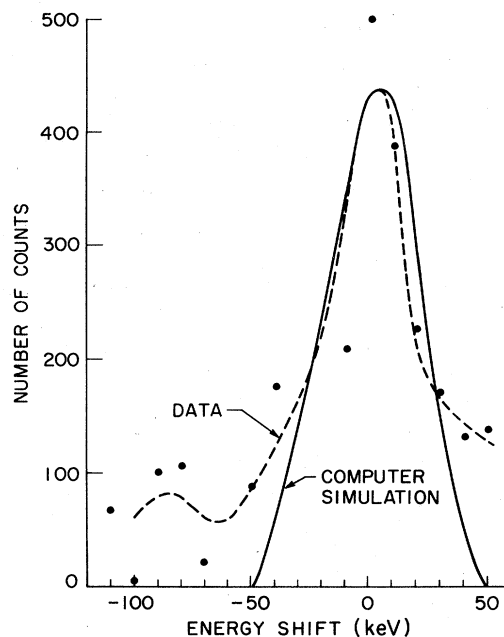


FIG. 5. Unmodulated electron energy spectrum. The dashed curve represents the data taken using hydrogen under the conditions listed in Table I. The electron-beam energy was 101.8 MeV. The solid curve was produced by the Monte Carlo computer simulation using the same parameters as the experiment; the peak was scaled to fit the data. Each data point represents an average of 2500 samples.

conditions as the data curve. The electron beam from the SCA has an intrinsic energy spread of ≈ 30 keV (FWHM). Resolution limits of the spectrometer magnet introduces ≈ 40 keV of uncertainty. Finally, the energy spread due to inelastic collisions with the windows and gas in the interaction region is ≈ 4 keV. Therefore, the total resolution is ≈ 50 keV.

A difference spectrum, generated by subtracting an unmodulated spectrum from a modulated spectrum, is shown in Fig. 6. The pressure was set to maximize the difference spectrum, i.e., this corresponded to the Čerenkov angle equaling the electron-laser intersection angle. The negative dip in the curve represents an $\approx 7\%$ reduction in the number of electrons in the central channels of the modulated spectrum. Allowing for the temporal overlap mismatch, $\approx 60\%$ of the electrons are removed by the laser pulse from the center of the spectrum.

The error bars represent one standard deviation assuming a normal distribution. A large noise source was electron-beam current fluctuations. Intensity fluctuations of the beam were caused by variations in the pulse-to-pulse current and spatial instability that resulted in the beam being clipped as it traversed through the windows in the gas cell. Other noise sources were laser and accelerator

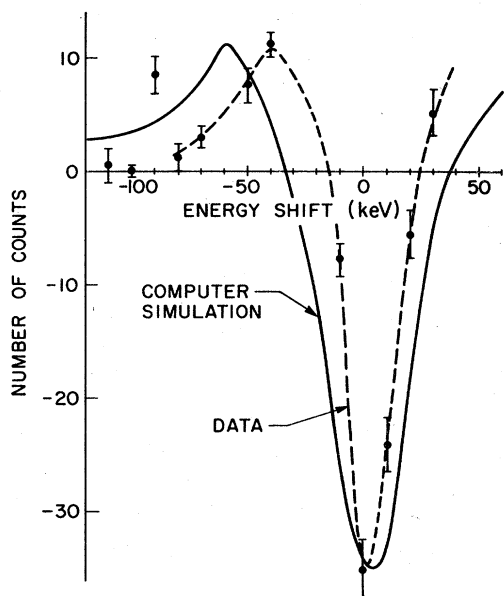


FIG. 6. Difference electron energy spectrum. The dashed curve is the data for hydrogen under the conditions given in Table I. The hydrogen pressure was 1.28 atm and corresponded to the Čerenkov angle equaling the electron-laser intersection angle. The solid curve represents the computer simulation for the same experimental conditions; the peak was scaled to fit the data.

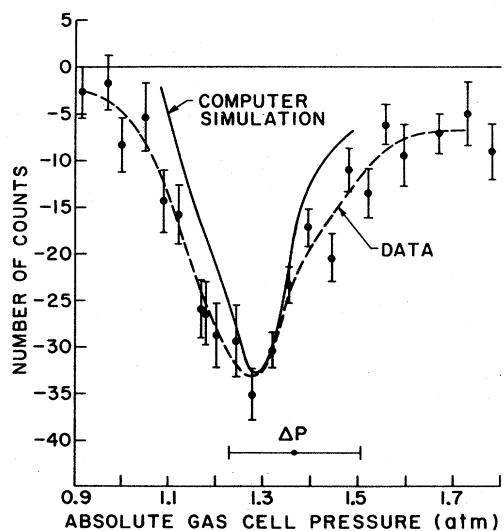


FIG. 7. Pressure dependence of interaction for hydrogen. Plotted is the average of the peak two channels of the difference spectra at each pressure. The pressure range ΔP shown on the bottom of the graph corresponds to an 18 ± 1 -mrad intersection angle as determined by the Čerenkov condition. The solid curve is the computer simulation of the dependence; the peak was scaled to fit the data. The electron-beam energy was 101.8 MeV.

electronic noise, and background radiation.

The solid curve in Fig. 6 is the difference spectrum generated by the computer program. The positive sidelobes of the experimental data are not clearly discernable due to noise, although the positive sidelobes of the Monte Carlo computer simulation predict the maximum energy exchange is ≈ 213 keV. This corresponds to a net average acceleration gradient of ≈ 3 MeV/m over 7 cm. To verify that the interaction is the result of the inverse Čerenkov effect, the Čerenkov condition must be varied from the optimal condition $\theta = \cos^{-1}(1/n\beta)$. This was done experimentally by varying the pressure and therefore the index of refraction.

Figure 7 shows the peak of the difference spectrum, obtained from an average of the peak two channels in the spectrum, as a function of pressure. Each data point was normalized to the beam current, and represents between 500 and 1500 samples. The dashed curve was obtained by a five-point least-squares parabolic fit to the data.

Similar results for the methane gas are shown in Fig. 8, plotted in the same manner as for hydrogen gas. The error bars are larger because the signal was weaker (due to more scattering and high background noise) and only 500 samples were

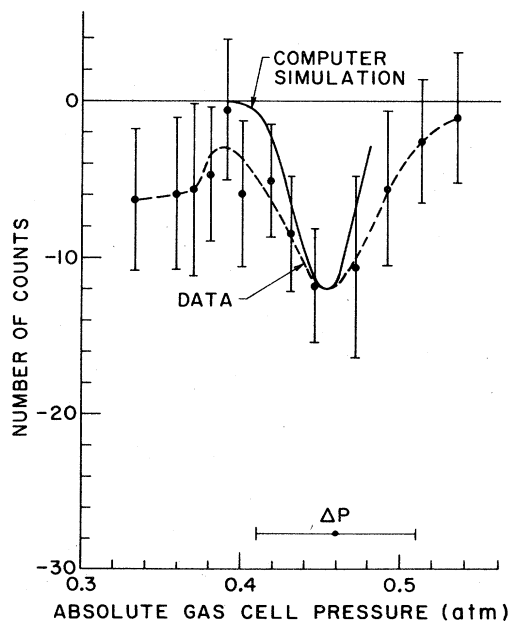


FIG. 8. Pressure dependence of interaction for methane. This was plotted in the same manner as Fig. 7. The pressure range ΔP indicated on the bottom of the graph corresponds to an 18 ± 1 -mrad intersection angle as determined by the Čerenkov condition. The computer simulation of the dependence is given by the solid curve; the peak was scaled to fit the data. The electron-beam energy was 101.8 MeV.

taken at each data point. Diminished energy exchange was expected as electron scattering is more severe for the higher average atomic charge of the methane molecule.

A strong indication that the observed effects were from the inverse Čerenkov interaction was that the peak dip in the hydrogen pressure curve occurred at 1.28 ± 0.04 atm, corresponding to a Čerenkov angle of 17.4 ± 0.3 mrad. This agreed, within experimental uncertainty, with the geometrically measured intersection angle of 18 ± 1 mrad. Also, the peak dip in the methane pressure curve occurred at 0.45 ± 0.03 atm, corresponding to a Čerenkov angle of 17.7 ± 0.6 mrad; again this agreed, within experimental error, with the Čerenkov condition.

Hydrogen was also investigated at a different electron-beam energy of 86.5 MeV, and at a slightly different intersection angle of 18.3 ± 1 mrad. Optimum energy exchange occurred at a pressure of 1.56 ± 0.04 atm, corresponding to a Čerenkov angle of 19 ± 0.3 mrad. Within experimental uncertainty, this again agreed with the measured intersection angle.

For hydrogen, at an electron beam energy of 101.8 MeV, a $\pm 13\%$ (± 0.16 atm) change in the gas pressure around the optimal pressure, reduced the interaction by one-half. The width of the pressure curve is largely determined by the electron- and laser-beam divergences, and to a lesser degree, by the electron energy spread and beam width. The solid curve shown in Fig. 7 is the computer simulation of the pressure dependence using the parameters listed in Table I. Although the simulation predicts a narrower dependence curve, this can be attributed to an uncertainty in the electron-beam divergence and width.

It was much more difficult to accurately determine the width of the methane pressure curve because of the substantial error bars. Approximately $\pm 8\%$ (± 0.04 atm) change in the gas pressure around the optimal pressure reduced the interaction by one-half. This variation could be as low as $\pm 3\%$ or as high as $\pm 12\%$ and be within the error bars. The solid curve represents the computer simulation of the pressure dependence for methane. Again, differences between the simulation and data can be attributed to uncertainties in the electron-beam quality.

IV. DISCUSSION

The inverse Čerenkov effect is an alternative method to the free electron laser (FEL)²⁰ for energy exchange between relativistic electrons and laser light. Bunching of the electrons as a

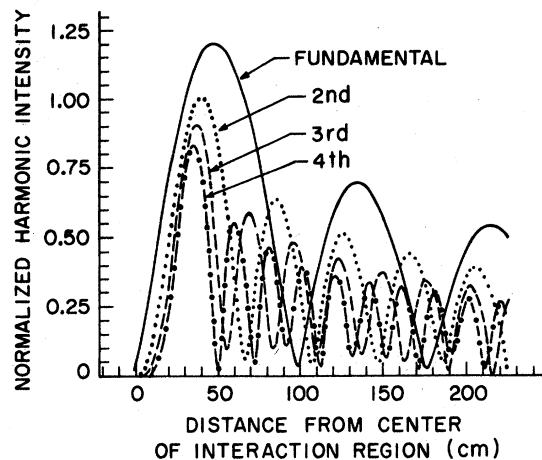


FIG. 9. Computer simulation of the electron-beam spatial harmonics as a result of laser-induced momentum modulation. Neglected in this idealized simulation were the effects of collisions, electron-beam width and divergence, and electron-beam energy spread. The first four harmonics of the beam are plotted normalized to the beam current and as a function of the distance from the center of the interaction region.

result of momentum modulation can occur, with the bunched beam containing spatial harmonics at integral multiples of the laser frequency. Figure 9 shows the spatial harmonic components varying as a function of distance from the center of the interaction region; this was produced by the Monte Carlo computer simulation using the parameters of this experiment but neglecting collisions, electron-beam width and beam divergence, and electron energy spread. Plotted vertically is the intensity of each harmonic component normalized to the beam current. Optimum bunching at the laser wavelength occurs ≈ 47 cm downstream from the interaction. At the peak, the harmonic component is 1.2 times the beam current, the second harmonic is 1.0 times, and the third harmonic is 0.7 times.

A bunched beam in a medium with the proper index of refraction will radiate electromagnetic energy in the form of enhanced Čerenkov light at the harmonic frequencies.^{21,22} This would create the optical analog of a microwave klystron. Stimulated Čerenkov emission can be produced from the bunched beam, providing a high-gain medium at the laser harmonics.

Considering the possibility of laser-induced particle accelerators, for the parameters of this experiment, the maximum energy exchange is ≈ 200 keV. This is for a single transit of the electron beam through the laser beam. Multiple passes will increase the amount of maximum energy exchange in proportion to the number of transits,

assuming phase stability between passes.

In conclusion, the inverse Čerenkov effect was demonstrated between a free electron beam and laser light. Changes in the electron energy and the pressure dependence of the interaction were measured using different phase-matching gases. The inverse Čerenkov effect was demonstrated and supported experimentally in two ways. First, the change in the electron energy spectrum was the greatest when the Čerenkov condition was satisfied. Second, the effect was a function of the index of refraction but independent of other parameters of the medium, as demonstrated with the use of two very different gases.

ACKNOWLEDGMENTS

The authors wish to thank Professor H. A. Schwettman and the staff at Stanford's High-Energy Physics Laboratory for their support of this experiment. They appreciate the helpful discussions and assistance of Dr. T. I. Smith, Dr. J. M. J. Madey, Dr. G. B. Rothbart, Dr. J. R. Calarco, and Dr. R. E. Rand, and acknowledge the useful conversations with Dr. J. R. Fontana and Dr. W. Zakowicz. This work was supported by the U. S. Office of Naval Research Contract No. N00014-78-C-0403, the U. S. Department of Energy Contract No. EY-76-S-0326, and by National Science Foundation Contract No. NSF-ENG76-11244.

-
- ¹K. Shimoda, *Appl. Opt.* **1**, 33 (1962).
²M. J. Feldman and R. Y. Chiao, *Phys. Rev. A* **4**, 352 (1971).
³P. K. Kaw and R. M. Kulsrud, *Phys. Fluids* **16**, 321 (1973).
⁴J. D. Lawson, Rutherford Laboratory Report No. RL-75-043, 1975 (unpublished).
⁵W. J. Willis, CERN publication, CERN 75, 1975 (unpublished).
⁶M. A. Piestrup, G. B. Rothbart, R. N. Fleming, and R. H. Pantell, *J. Appl. Phys.* **46**, 132 (1975).
⁷W. D. Kimura, R. H. Pantell, M. A. Piestrup, and G. B. Rothbart, *Progress in Astronautics and Aeronautics* (American Institute of Aeronautics and Astronautics, New York, 1978), Vol. 61, pp. 368-378.
⁸R. H. Pantell and M. A. Piestrup, *Appl. Phys. Lett.* **32**, 781 (1978).
⁹J. A. Edighoffer and R. H. Pantell, *J. Appl. Phys.* **50**, 6120 (1979).
¹⁰R. H. Pantell and J. A. Edighoffer, *J. Appl. Phys.* **51**, 1905 (1980).
¹¹A. H. Beck and P. Chung, Proceeding of the Fourth European Microwave Conference, Montreuz, Switzerland, 1974, pp. 405-409 (unpublished).
¹²K. Mizuno and S. Ono, *Proc. IEEE* **63**, 1075 (1975).
¹³J. E. Walsh, T. C. Marshall, and S. P. Schlesinger, *Phys. Fluids* **20**, 4709 (1977).
¹⁴A. Gover and A. Yariv, *Appl. Phys.* **16**, 121 (1978).
¹⁵J. E. Walsh, *Physics of Quantum Electronics*, edited by S. Jacobs, M. Sargent, and M. Scully (Addison-Wesley, Reading, Mass., 1978), Vol. 5.
¹⁶M. A. Piestrup, Ph.D. dissertation, Stanford University, 1972 (unpublished).
¹⁷C. K. Chen, J. C. Sheppard, M. A. Piestrup, and R. H. Pantell, *J. Appl. Phys.* **49**, 41 (1978).
¹⁸N. A. Korkhmazyun, L. A. Gevorgyan, and M. L. Petrosyan, *Zh. Tekh. Fiz.* **47**, 1583 (1977) [*Sov. Phys.—Tech. Phys.* **22**, 917 (1977)].
¹⁹M. I. Dyakonov and D. A. Varshalovich, *Phys. Lett.* **35**, 277 (1971).
²⁰L. R. Elias, W. M. Fairbank, J. M. Madey, H. A. Schwettman, and T. I. Smith, *Phys. Rev. Lett.* **36**, 717 (1976).
²¹H. Lashinsky, *Advances in Electronics and Electron Physics*, edited by L. Marton (Academic, New York, 1961), Vol. XIV, p. 265.
²²P. D. Coleman and C. Enderby, *J. Appl. Phys.* **31**, 1695 (1960).